

Contents

Abstract (in Chinese)	i
Abstract (in English)	iv
Acknowledgments (in Chinese)	ix
Contents	x
Table Lists	xv
Figure Captions	xvii

Chapter 1 Introduction.....1

1.1 Overview of Low-Temperature Polycrystalline Silicon Thin-Film Transistors (LTPS TFT) Technology.....	1
1.2 Overview of Key Processes in the Fabrication of LTPS TFTs.....	3
1.2.1 Crystallization of Amorphous Silicon Thin Films.....	4
1.2.1.1 Solid Phase Crystallization.....	6
1.2.1.1.1 Solid Phase Crystal of Pure Amorphous Silicon.....	6
1.2.1.1.2 Metal Induced (Lateral) Crystallization.....	7
1.2.1.2 Liquid Phase Crystallization (Laser Crystallization).....	10
1.2.2 Gate Dielectric Formation.....	12
1.2.3 Impurity Doping and Low-Thermal-Budge Activation.....	14
1.3 Electrical Characteristics of LTPS TFTs.....	17
1.4 System on Panel (SOP) Issues in LTPS TFTs.....	19
1.5 Motivation.....	21
1.5.1 From the Perspective of Channel Material – Enhance the Field-Effect Mobility by Adding Germanium Atoms into the Poly-Si Active Layer.....	22
1.5.2 From the Perspective of Crystallization Structure – Enhance the Field-Effect	

Mobility and Improve the Device Uniformity by Using a-Si-Sapcer-Aided Location-Controlled Lateral Laser Crystallization.....	23
1.6 Thesis Organization.....	24

Chapter 2 Process and Device Characterizations of Low-Temperature Polycrystalline Silicon Thin Film Transistors27

2.1 Introduction.....	27
2.2 Excimer Laser Crystallization of a-Si Thin Film.....	30
2.2.1 Heat Transport and Grain Growth Mechanism of Excimer-Laser-Annealed Poly-Si Thin Films.....	30
2.2.2 Experimental Procedure.....	35
2.2.2.1 The Excimer Laser Crystallization System.....	35
2.2.2.2 Sample Preparation for Material Analysis.....	37
2.2.2.3 Fabrication of ELC LTPS TFTs.....	37
2.2.3 Results and Discussion.....	39
2.2.3.1 Material Characterization of ELC Poly-Si Thin Films.....	39
2.2.3.1.1 Scanning Electron Microscopy (SEM) Analysis.....	39
2.2.3.1.2 Atomic Force Microscopy (AFM) Analysis.....	43
2.2.3.2 Electrical Characterization of ELC LTPS TFT.....	46
2.2.3.3 Short Channel Effect of ELC LTPS TFTs.....	52
2.3 Deposition and Reliability Analysis of Low-Temperature Gate Dielectric.....	59
2.3.1 Low-Temperature Deposition of SiO ₂ Thin Film.....	59
2.3.2 Experimental Procedure.....	60
2.3.2.1 Low-Temperature SiO ₂ Thin Film Deposition.....	60
2.3.2.2 Post Plasma Treatment of SiO ₂ Thin Film.....	61

2.3.3 Results and Discussion.....	63
2.3.3.1 Low-temperature SiO ₂ Thin Film.....	63
2.3.3.2 Long-Term Reliability of Post-Plasma-Treated SiO ₂ Thin Film.....	65
2.4 Summary.....	69

Chapter 3 Process and Device Characterizations of Low-Temperature Polycrystalline Silicon-Germanium (poly-Si_{1-x}Ge_x) Thin Film Transistors.....71

3.1 Introduction.....	71
3.2 Experimental Procedure.....	76
3.2.1 a-Si _{1-x} Ge _x Thin Film Deposition.....	76
3.2.2 Excimer Laser Crystallization of a-Si _{1-x} Ge _x Thin Films.....	77
3.2.3 Fabrication of Low-Temperature Poly-Si _{1-x} Ge _x TFTs Using ELC.....	78
3.3 Material Characterization of Si _{1-x} Ge _x Thin Films.....	80
3.3.1 Deposition Characterization of a-Si _{1-x} Ge _x Thin Films.....	80
3.3.2 Material Characterization of ELC Poly-Si _{1-x} Ge _x Thin Films.....	86
3.3.2.1 X-Ray Diffraction (XRD) Analysis.....	86
3.3.2.2 Raman Spectroscopy Analysis.....	89
3.3.2.3 Auger Electron Spectroscopy (AES) Analysis.....	92
3.3.2.4 Transmission Electron Microscopy (TEM) Analysis.....	96
3.3.2.5 Scanning Electron Microscope (SEM) Analysis.....	100
3.4 The Crystallization Mechanism of Excimer-Laser-Irradiated a-Si _{1-x} Ge _x Thin Films.....	106
3.5 Electrical Characterization of ELC poly-Si _{1-x} Ge _x TFTs.....	108
3.6 Summary.....	114

Chapter 4 Fabrication of Low-Temperature Polycrystalline Silicon-Germanium Thin Film Transistors by Using a Novel Germanium Doping Method.....116

4.1 Introduction.....116

4.2 Experimental Procedure.....119

 4.2.1 Fabrication of ELC Poly-Si_{1-x}Ge_x TFTs with Si capping Layer.....119

 4.2.2 Fabrication of Ge-Doped ELC Poly-Si_{1-x}Ge_x TFTs.....122

4.3 Results and Discussion.....125

 4.3.1 Characterizations of ELC poly- Si_{1-x}Ge_x TFTs with Si capping layer.....125

 4.3.1.1 The Principle of Controlled Ge Segregation.....125

 4.3.1.2 Electrical Characterization of ELC Poly-Si_{1-x}Ge_x TFTs with Si Capping Layer.....126

 4.3.2 Characterization of Ge-Doped ELC Poly- Si_{1-x}Ge_x TFTs.....132

 4.3.2.1 The Improvement of Thin Film Crystallinity and Controlled Ge Segregation.....132

 4.3.2.2 Electrical Characterization of Ge-Doped ELC poly-Si_{1-x}Ge_x TFTs.....135

4.4 Summary.....152

Chapter 5 High-Performance Polycrystalline Silicon Thin Film Transistors Crystallized by Excimer Laser Irradiation with a-Si Spacer Structure.....155

5.1 Introduction.....155

5.2. The Concept of Periodic Lateral Grain Growth with a-Si Spacer Structure.....158

5.3 Experimental Procedure.....162

 5.3.1 Sample Preparation for SEM Observation.....162

 5.3.2 Fabrication of Small Dimension Poly-Si TFT with a-Si Spacer Structure.....164

5.3.3 Fabrication of Large Dimension Poly-Si TFT with a-Si Spacer Structure.....	166
5.4 Results and Discussion.....	168
5.4.1 Material Analysis of Poly-Si Thin Film with Periodic Lateral Grain Growth.	168
5.4.2 Electrical Characteristics of Small Dimension Poly-Si Thin Film Transistors with a-Si Spacer Structure.....	182
5.4.2.1 a-Si Spacer with a Thickness of 1500Å.....	182
5.4.2.1 a-Si Spacer with a Thickness of 2000Å.....	191
5.4.3 Electrical Characteristics of Large Dimension Poly-Si Thin Film Transistors with a-Si Spacer Structure.....	197
5.4.3.1 a-Si Spacer with a Thickness of 1500Å.....	197
5.4.3.2 a-Si Spacer with a Thickness of 2000Å.....	211
5.5 Summary.....	225
Chapter 6 Summary and Conclusions.....	226
Chapter 7 Future Prospects.....	231
References.....	234



Vita

Publication Lists

Table Lists

Chapter 2

Table 2.1 Plasma treatment parameters.

Table 2.2 Electrical characteristics of the TEOS oxide deposited by LA-PECVD.

Chapter 3

Table 3.1 Detailed deposition parameters of LPCVD $\text{Si}_{1-x}\text{Ge}_x$ Thin Film.

Table 3.2 The detail relationship between the deposition parameters and the crystalline phase.

Table 3.3 The electrical characteristic of p-channel poly- $\text{Si}_{0.77}\text{Ge}_{0.23}$ and poly-Si TFTs.



Chapter 4

Table 4.1 Measured electrical characteristics of p-channel ELC poly-Si TFTs and Si-capped poly- $\text{Si}_{1-x}\text{Ge}_x$ TFTs after 4-h NH_3 plasma treatment.

Table 4.2 Measured electrical characteristics of n-channel ELC poly-Si TFTs and Ge-doped ELC poly- $\text{Si}_{1-x}\text{Ge}_x$ TFTs before NH_3 plasma treatment.

Table 4.3 Measured electrical characteristics of p-channel ELC poly-Si TFTs and Ge-doped ELC poly- $\text{Si}_{1-x}\text{Ge}_x$ TFTs before NH_3 plasma treatment.

Table 4.4 Measured electrical characteristics of n-channel ELC poly-Si TFTs and Ge-doped ELC poly- $\text{Si}_{1-x}\text{Ge}_x$ TFTs after 4-h NH_3 plasma treatment.

Table 4.5 Measured electrical characteristics of p-channel ELC poly-Si TFTs and Ge-doped ELC poly- $\text{Si}_{1-x}\text{Ge}_x$ TFTs after 4-h NH_3 plasma treatment.

Chapter 5

- Table 4.1 Measured optimal electrical characteristics of TFTs crystallized with a-Si spacer and conventional structure. The a-Si spacer thickness is 1500Å.
- Table 4.2 Measured optimal electrical characteristics of TFTs crystallized with a-Si spacer and conventional structure. The a-Si spacer thickness is 2000Å.
- Table 4.3 Measured optimal electrical characteristics of TFTs crystallized with conventional and a-Si spacer structure, in which the distances between neighboring a-Si spacers are 1 μm , 1.5 μm , 2 μm , 2.5 μm , 3 μm , and 4 μm , respectively. The device channel length and width are 10 μm . The a-Si spacer thickness is 1500Å.
- Table 4.4 Measured optimal electrical characteristics of TFTs crystallized with conventional and a-Si spacer structure, in which the distances between neighboring a-Si spacers are 1 μm , 2 μm , 2.5 μm , 3 μm , and 4 μm , respectively.
- Table 4.5 Measured optimal electrical characteristics of TFTs crystallized with conventional and a-Si spacer structure, in which the distances between neighboring a-Si spacers are 1 μm , 1.5 μm , 2 μm , 2.5 μm , 3 μm , and 4 μm , respectively. The device channel length and width are 10 μm . The a-Si spacer thickness is 2000Å.
- Table 4.6 Measured optimal electrical characteristics of TFTs crystallized with conventional and a-Si spacer structure, in which the distances between neighboring a-Si spacers are 1 μm , 2 μm , 2.5 μm , 3 μm , and 4 μm , respectively.

Figure Captions

Chapter 2

- Figure 2.1 The schematic view of the recrystallization mechanism in the partial melting regime.
- Figure 2.2 The schematic view of the recrystallization mechanism in the full melting regime.
- Figure 2.3 The schematic illustration of the recrystallization mechanism in the super lateral growth (SLG) regime.
- Figure 2.4 The brief schematic of excimer laser crystallization system.
- Figure 2.5 The key processes for fabrication of the ELC LTPS TFTs.
- Figure 2.6 SEM graph of the 500Å poly-Si thin film crystallized in the (a) partial melting regime. (b) SLG regime. (c) full melting regime.
- Figure 2.7 SEM graph of the 1000Å poly-Si thin film crystallized in the (a) partial melting regime. (b) SLG regime. (c) full melting regime.
- Figure 2.8 SEM graph of the poly-Si thin film crystallized in the SLG regime. (a) 500Å (b) 1000Å
- Figure 2.9 AFM image of the 1000Å poly-Si thin film crystallized in the (a) partial melting regime. (b) SLG regime. (c) full melting regime.
- Figure 2.10 The dependence of (a) field-effect mobility and (b) threshold voltage of LTPS TFTs with 500Å-thick active layer on the applied laser energy density for ELC performing at room temperature.
- The dependence of (c) field-effect mobility and (d) threshold voltage of LTPS TFTs with 500Å-thick active layer on the applied laser energy density for ELC performing at 400°C.

Figure 2.11 The dependence of (a) field-effect mobility and (b) threshold voltage of LTPS TFTs with 1000Å-thick active layer on the applied laser energy density for ELC performing at room temperature.

The dependence of (c) field-effect mobility and (d) threshold voltage of LTPS TFTs with 1000Å-thick active layer on the applied laser energy density for ELC performing at 400°C.

Figure 2.12 The dependence of (a) field-effect mobility and (b) threshold voltage of LTPS TFTs with 500Å-thick active layer on the device dimension for ELC performed at room temperature.

The dependence of (c) field-effect mobility and (d) threshold voltage of LTPS TFTs with 500Å-thick active layer on the device dimension for ELC performed at 400°C.

Figure 2.13 The dependence of (a) field-effect mobility and (b) threshold voltage of LTPS TFTs with 1000Å-thick active layer on the device dimension for ELC performed at room temperature.

The dependence of (c) field-effect mobility and (d) threshold voltage of LTPS TFTs with 1000Å-thick active layer on the device dimension for ELC performed at 400°C.

Figure 2.14 The key fabrication process of the MOS capacitors.

Figure 2.15 The key fabrication process of the plasma-treated MOS capacitors.

Figure 2.16 The cross-section TEM graphs of as-deposited TEOS oxide (a) X300K. (b) X50K.

Figure 2.17 The capacitance-voltage (C-V) characteristic of the as-deposited TEOS oxide.

Figure 2.18 Time-zero dielectric breakdown Characteristics of TEOS oxide as a function of treatment time under different plasma ambient.

Figure 2.19 Charge-to-breakdown characteristics of TEOS oxide as a function of treatment

time under different plasma ambient.

Figure 2.20 Bias temperature instability characteristics of TEOS oxide as a function of treatment time with NH_3 & N_2O plasma ambient.

Chapter 3

Figure 3.1 The key process procedure of fabricating ELC poly- $\text{Si}_{1-x}\text{Ge}_x$ TFTs.

Figure 3.2 XRD spectrum of as-deposited LPCVD $\text{Si}_{1-x}\text{Ge}_x$ thin film.

Figure 3.3 $\text{Si}_{1-x}\text{Ge}_x$ thin film deposition rate as a function of temperature with different $\text{SiH}_4/\text{GeH}_4$ gas flow ratio.

Figure 3.4 The relationship between the Ge atomic concentration and $\text{GeH}_4/\text{SiH}_4$ gas flow ratio for two deposition temperatures of 450°C and 470°C .

Figure 3.5 XRD spectrum of ELC $\text{Si}_{0.77}\text{Ge}_{0.23}$ thin film irradiated at room temperature.

Figure 3.6 XRD spectrum of ELC $\text{Si}_{0.67}\text{Ge}_{0.33}$ thin film irradiated at room temperature.

Figure 3.7 XRD spectrum of ELC $\text{Si}_{0.77}\text{Ge}_{0.23}$ thin film irradiated at 400°C .

Figure 3.8 Raman spectra of ELC $\text{Si}_{0.77}\text{Ge}_{0.23}$ thin films irradiated with different laser energy density at room temperature.

Figure 3.9 Raman spectra of ELC $\text{Si}_{0.67}\text{Ge}_{0.33}$ thin films irradiated with different laser energy density at room temperature.

Figure 3.10 Raman spectra of ELC $\text{Si}_{0.67}\text{Ge}_{0.33}$ thin films irradiated with different shot numbers at room temperature. The laser energy density is 350 mJ/cm^2 .

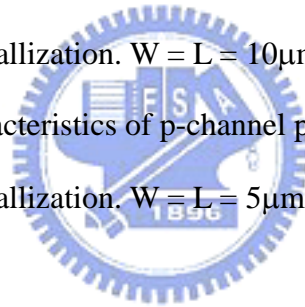
Figure 3.11 Raman spectra of ELC $\text{Si}_{0.67}\text{Ge}_{0.33}$ thin films irradiated with different shot numbers at room temperature. The laser energy density is 380 mJ/cm^2 .

Figure 3.12 AES depth profile of the as-deposited a- $\text{Si}_{0.77}\text{Ge}_{0.23}$ thin film.

Figure 3.13 AES depth profile of the ELC poly- $\text{Si}_{0.77}\text{Ge}_{0.23}$ with $E = 260 \text{ mJ/cm}^2$, 100 shots at R.T.

- Figure 3.14 AES depth profile of the ELC poly-Si_{0.77}Ge_{0.23} with E = 300 mJ/cm², 100 shots at R.T.
- Figure 3.15 AES depth profile of the ELC poly-Si_{0.77}Ge_{0.23} with E = 340 mJ/cm², 100 shots at R.T.
- Figure 3.16 AES depth profile of the ELC poly-Si_{0.77}Ge_{0.23} with E = 360 mJ/cm², 20 shots at R.T.
- Figure 3.17 AES depth profile of the ELC poly-Si_{0.77}Ge_{0.23} with E = 420 mJ/cm², 20 shots at R.T.
- Figure 3.18 Plain-view TEM micrographs and diffraction pattern of the ELC poly-Si_{0.77}Ge_{0.23} thin films. E = 300mJ/cm², 100 shots at R.T.
- Figure 3.19 Cross-section TEM micrographs and EDX analysis results of the (a) as-deposited a-Si_{0.77}Ge_{0.23} thin film. (b) ELC poly-Si_{0.77}Ge_{0.23} thin film. E = 300mJ/cm², 100 shots at R.T.
- Figure 3.20 The SEM micrographs of the ELC poly-Si_{1-x}Ge_x film after Secco etching. E = (a) 350mJ/cm² (b) 370 mJ/cm² (c) 390 mJ/cm² (d) 410 mJ/cm².
- Figure 3.21 SEM micrographs of ELC poly-Si_{0.77}Ge_{0.23} films irradiated at R.T. after modified Secco etching treatment. (a) 350mJ/cm², 100shots (b) 350mJ/cm², 20shots (c) 390mJ/cm², 100shots (d) 390mJ/cm², 20shots (e) 410mJ/cm², 100shots (f) 410mJ/cm², 20shots
- Figure 3.22 SEM micrographs of ELC poly-Si_{0.77}Ge_{0.23} films irradiated at 400°C after modified Secco etching treatment. (a) 350mJ/cm², 100shots (b) 350mJ/cm², 20shots (c) 390mJ/cm², 100shots (d) 390mJ/cm², 20shots (e) 410mJ/cm², 100shots (f) 410mJ/cm², 20shots
- Figure 3.23 SEM micrographs of ELC poly-Si_{0.67}Ge_{0.33} films irradiated at 400°C after modified Secco etching treatment. (a) 330mJ/cm², 100shots (b) 330mJ/cm², 20shots (c) 350mJ/cm², 100shots (d) 350mJ/cm², 20shots

- Figure 3.24 SEM images of ELC poly-Si and poly-Si_{0.77}Ge_{0.23} thin films crystallized with optimum laser conditions. The shot number is 100.
- Figure 3.25 The proposed crystallization model for poly-Si_{1-x}Ge_x films crystallized by excimer laser irradiation.
- Figure 3.26 Typical transfer characteristics of p-channel poly-Si_{0.77}Ge_{0.23} TFTs fabricated by excimer laser crystallization. W = L = 3μm.
- Figure 3.27 Typical transfer characteristics of p-channel poly-Si_{0.77}Ge_{0.23} TFTs fabricated by excimer laser crystallization. W = L = 5μm.
- Figure 3.28 Schematic illustration of the leakage mechanism model and band bending under applied bias in polysilicon thin-film transistors. Ref. [3.65]
- Figure 3.29 Typical output characteristics of p-channel poly-Si_{0.77}Ge_{0.23} TFTs fabricated by excimer laser crystallization. W = L = 10μm.
- Figure 3.30 Typical output characteristics of p-channel poly-Si_{0.77}Ge_{0.23} TFTs fabricated by excimer laser crystallization. W = L = 5μm.



Chapter 4

- Figure 4.1 The key fabrication process of ELC poly-Si_{1-x}Ge_x TFTs with Si capping layer.
- Figure 4.2 The key fabrication process of Ge-doped ELC poly-Si_{1-x}Ge_x TFTs.
- Figure 4.3 Typical transfer characteristics of p-channel poly-Si_{0.88}Ge_{0.12} TFTs fabricated by excimer laser crystallization of a-Si/poly-Si_{0.77}Ge_{0.23} structure. W = L = 10μm.
- Figure 4.4 Typical transfer characteristics of p-channel poly-Si_{0.88}Ge_{0.12} TFTs fabricated by excimer laser crystallization of a-Si/poly-Si_{0.77}Ge_{0.23} structure. W = L = 5μm.
- Figure 4.5 Typical transfer characteristics of p-channel poly-Si_{0.84}Ge_{0.16} TFTs fabricated by excimer laser crystallization of a-Si/poly-Si_{0.67}Ge_{0.33} structure. W = L = 10μm.
- Figure 4.6 Typical transfer characteristics of p-channel poly-Si_{0.84}Ge_{0.16} TFTs fabricated by

excimer laser crystallization of a-Si/poly-Si_{0.67}Ge_{0.33} structure. W = L = 5μm.

Figure 4.7 Typical output characteristics of p-channel poly-Si_{0.84}Ge_{0.16} TFTs fabricated by excimer laser crystallization of a-Si/poly-Si_{0.67}Ge_{0.33} structure. W = L = 10μm.

Figure 4.8 Typical output characteristics of p-channel poly-Si_{0.84}Ge_{0.16} TFTs fabricated by excimer laser crystallization of a-Si/poly-Si_{0.67}Ge_{0.33} structure. W = L = 5μm.

Figure 4.9 The RBS analysis results of the Ge-doped ELC poly-Si_{1-x}Ge_x thin films capped with (a) a-Si_{0.77}Ge_{0.23} and (b) a-Si_{0.67}Ge_{0.33} upper layers. The final Ge atomic concentration is equivalent to (a) 5% and (b) 9%, respectively.

Figure 4.10 The typical transfer characteristics of the conventional ELC n-channel poly-Si TFTs and the Ge-doped n-channel poly-Si_{0.95}Ge_{0.05} TFTs. W/L = 10μm/10μm.

Figure 4.11 The typical transfer characteristics of the conventional ELC n-channel poly-Si TFTs and the Ge-doped n-channel poly-Si_{0.95}Ge_{0.05} TFTs. W/L = 5μm/5μm.

Figure 4.12 The typical transfer characteristics of the conventional ELC p-channel poly-Si TFTs and the Ge-doped n-channel poly-Si_{0.95}Ge_{0.05} TFTs. W/L = 10μm/10μm.

Figure 4.13 The typical transfer characteristics of the conventional ELC p-channel poly-Si TFTs and the Ge-doped n-channel poly-Si_{0.95}Ge_{0.05} TFTs. W/L = 5μm/5μm.

Figure 4.14 The typical transfer characteristics of the conventional ELC p-channel poly-Si TFTs and the Ge-doped n-channel poly-Si_{0.91}Ge_{0.09} TFTs. W/L = 10μm/10μm.

Figure 4.15 The typical transfer characteristics of the conventional ELC p-channel poly-Si TFTs and the Ge-doped n-channel poly-Si_{0.91}Ge_{0.09} TFTs. W/L = 5μm/5μm.

Figure 4.16 The typical transfer characteristics of the conventional ELC n-channel poly-Si TFTs and the Ge-doped n-channel poly-Si_{0.95}Ge_{0.05} TFTs. W/L = 2μm/2μm.

Figure 4.17 The typical transfer characteristics of the conventional ELC n-channel poly-Si TFTs and the Ge-doped n-channel poly-Si_{0.95}Ge_{0.05} TFTs. W/L = 1.5μm/1.5μm.

Figure 4.18 The typical transfer characteristics of the conventional ELC p-channel poly-Si TFTs and the Ge-doped n-channel poly-Si_{0.95}Ge_{0.05} TFTs. W/L = 2μm/2μm.

- Figure 4.19 The typical transfer characteristics of the conventional ELC p-channel poly-Si TFTs and the Ge-doped n-channel poly-Si_{0.95}Ge_{0.05} TFTs. W/L = 1.5μm/1.5μm.
- Figure 4.20 The typical transfer characteristics of the conventional ELC p-channel poly-Si TFTs and the Ge-doped n-channel poly-Si_{0.91}Ge_{0.09} TFTs. W/L = 2μm/2μm.
- Figure 4.21 The typical transfer characteristics of the conventional ELC p-channel poly-Si TFTs and the Ge-doped n-channel poly-Si_{0.91}Ge_{0.09} TFTs. W/L = 1.5μm/1.5μm.
- Figure 4.22 The dependence of mobility on device dimension and Ge atomic concentration for (a) n-channel and (b) p-channel Ge-doped ELC poly-Si_{1-x}Ge_x TFTs.
- Figure 4.23 The output characteristics of the conventional p-channel ELC poly-Si TFTs and the Ge-doped p-channel poly-Si_{0.95}Ge_{0.05} TFTs.
- Figure 4.24 The output characteristics of the conventional p-channel ELC poly-Si TFTs and the Ge-doped p-channel poly-Si_{0.91}Ge_{0.09} TFTs.
- Figure 4.25 The n-channel transfer characteristics of the conventional ELC poly-Si TFTs and the Ge-doped poly-Si_{0.95}Ge_{0.05} TFTs after 4-h NH₃ plasma treatment. W = L = 2μm.
- Figure 4.26 The p-channel transfer characteristics of the conventional ELC poly-Si TFTs and the Ge-doped poly-Si_{0.95}Ge_{0.05} TFTs after 4-h NH₃ plasma treatment. W=L = 2μm.

Chapter 5

- Figure 5.1 The schematic illustration of lateral grain growth mechanism using an a-Si spacer structure.
- Figure 5.2 The schematic illustration of relative location of the channel region and amorphous Si spacer seed.
- Figure 5.3 The schematic illustration of the periodic grain growth with a-Si spacer

structure.

- Figure 5.4 The process procedure of producing periodic lateral grain growth.
- Figure 5.5 The key processes for fabrication of the poly-Si TFTs crystallized with a-Si spacer structure.
- Figure 5.6 The schematic illustration of the relative positions of the channel region and the a-Si spacer location for large-size device.
- Figure 5.7 The key processes for fabrication of the large-dimension poly-Si TFTs crystallized with a-Si spacer structure.
- Figure 5.8 SEM picture of excimer laser crystallized poly-Si with 1500Å-thick a-Si spacer structure. The distance between adjacent a-Si spacers is 1 μm
- Figure 5.9 SEM graph of the crystallized poly-Si thin film, in which the length of the adjacent a-Si spacers is 2 μm.
- Figure 5.10 SEM graph of the crystallized poly-Si thin film. in which the length of the adjacent a-Si spacers is 2 μm. The applied laser energy density is (a) 410 mJ/cm². (b) 435 mJ/cm². (c) 460 mJ/cm². (d) 485 mJ/cm².
- Figure 5.11 SEM graph of the crystallized poly-Si thin film. in which the length of the adjacent a-Si spacers is 2 μm. The applied laser energy density is (a) 10 mJ/cm². (b) 535 mJ/cm². (c) 560 mJ/cm². (d) 585 mJ/cm².
- Figure 5.12 AFM images of the Si thin film with 1500Å-thick spacer heights before laser irradiation (a) flat image (b) 3-D image
- Figure 5.13 AFM images of the Si thin film with 1500Å-thick spacer heights after laser irradiation (a) flat image (b) 3-D image.
- Figure 5.14. AFM images of the Si thin film with 2000Å-thick spacer heights before laser irradiation (a) flat image (b) 3-D image.
- Figure 5.15 AFM images of the Si thin film with 2000Å-thick spacer heights after laser irradiation (a) flat image (b) 3-D image.

- Figure 5.16 The crystallization mechanism of the poly-Si thin film with 2000Å-thick a-Si spacer.
- Figure 5.17 The typical transfer characteristic of poly-Si TFTs crystallized using a-Si spacer structure with channel length of (a) 1.5 μm (b) 2 μm (c) 3 μm (d) 4 μm (e) 5 μm, in which the thickness of a-Si spacer is 1500Å.
- Figure 5.18 The output characteristic of poly-Si TFTs crystallized using a-Si spacer structure with channel length of (a) 1.5 μm (b) 2 μm (c) 3 μm (d) 4 μm (e) 5 μm. The a-Si spacer thickness is 1500Å.
- Figure 5.19 The dependence of field-effect mobility on the applied laser energy density for poly-Si TFTs crystallized with a-Si spacer and conventional structures.
- Figure 5.20 The typical transfer characteristic of poly-Si TFTs crystallized using a-Si spacer structure with channel length of (a) 1.5 μm (b) 2 μm (c) 3 μm (d) 4 μm (e) 5 μm, in which the thickness of a-Si spacer is 2000Å.
- Figure 5.21 The output characteristic of poly-Si TFTs crystallized using a-Si spacer structure with channel length of (a) 1.5 μm (b) 2 μm (c) 3 μm (d) 4 μm (e) 5 μm. The a-Si spacer thickness is 2000Å.
- Figure 5.22 The typical transfer characteristics of poly-Si TFTs crystallized using 1500Å-thick a-Si spacer structure with channel length of 10 μm, in which the distances between neighboring a-Si spacers are (a) 1 μm (b) 1.5 μm (c) 2 μm (d) 2.5 μm (e) 3 μm (f) 4 μm .
- Figure 5.23 The output characteristics of ELC poly-Si TFTs crystallized using 1500Å-thick a-Si spacer structure with channel length of 10 μm, in which the distances between neighboring a-Si spacers are (a) 1 μm (b) 1.5 μm (c) 2 μm (d) 2.5 μm (e) 3 μm (f) 4 μm .
- Figure 5.24 The typical transfer characteristics of poly-Si TFTs crystallized using 1500Å-thick a-Si spacer structure with channel length of 20 μm, in which the

distances between neighboring a-Si spacers are (a) 1 μm (b) 2 μm (c) 2.5 μm (d) 3 μm (e) 4 μm .

Figure 5.25 The output characteristics of ELC poly-Si TFTs crystallized using 1500 \AA -thick a-Si spacer structure with channel length of 20 μm , in which the distances between neighboring a-Si spacers are (a) 1 μm (b) 2 μm (c) 2.5 μm (d) 3 μm (e) 4 μm .

Figure 5.26 The typical transfer characteristics of poly-Si TFTs crystallized using 2000 \AA -thick a-Si spacer structure with channel length of 10 μm , in which the distances between neighboring a-Si spacers are (a) 1 μm (b) 1.5 μm (c) 2 μm (d) 2.5 μm (e) 3 μm (f) 4 μm .

Figure 5.27 The output characteristics of ELC poly-Si TFTs crystallized using 2000 \AA -thick a-Si spacer structure with channel length of 10 μm , in which the distances between neighboring a-Si spacers are (a) 1 μm (b) 1.5 μm (c) 2 μm (d) 2.5 μm (e) 3 μm (f) 4 μm .

Figure 5.28 The typical transfer characteristics of poly-Si TFTs crystallized using 2000 \AA -thick a-Si spacer structure with channel length of 20 μm , in which the distances between neighboring a-Si spacers are (a) 1 μm (b) 2 μm (c) 2.5 μm (d) 3 μm (e) 4 μm .

Figure 5.29 The output characteristics of ELC poly-Si TFTs crystallized using 2000 \AA -thick a-Si spacer structure with channel length of 20 μm , in which the distances between neighboring a-Si spacers are (a) 1 μm (b) 2 μm (c) 2.5 μm (d) 3 μm (e) 4 μm .